Theory of two-photon Lamb dips

Fujio Shimizu*
Division of Physics, National Research Council of Canada, Ottawa, Ontario, Canada
(Received 28 March 1974)

A semiclassical theory of two-photon Lamb dips is presented, when one of the radiations is in the radio-frequency region and the other is in the optical region. Perturbation solutions as well as an exact recurrence formula are discussed. For the latter case numerical results are given. The resonance line shape of the two-photon Lamb dip shows a variety of changes according to the experimental conditions. When both the optical and the rf fields are weak a line is of a dispersion form. When the rf field is increased, the line changes to a Lorentzian form. When the optical field is increased, the line is shifted and broadened. If the radio frequency is close to or less than the Doppler width of the gas, a two-photon Lamb dip is accompanied with satellite dips which correspond to molecules with nonzero velocity components along the propagation of the laser radiation. The intensity of a two-photon Lamb dip is expected to decrease rapidly with increasing radio frequency. Additional effects when the sample cell is placed inside the laser cavity are also discussed. Those results agree qualitatively with recent observations by Freund, Römheld, and Oka.

I. INTRODUCTION

The recent observation of two-photon Lamb dips by Freund and Oka[1] demonstrates a convenient method for accurate determination of molecular-transition frequencies which are not in coincidence with standard laser lines. By using a nonlinearity of molecular-transition processes, a radio frequency is added to or subtracted from the laser frequency. If the laser frequency is accurately known, this technique is much simpler than the standard Lamb-dip measurement combined with a tunable laser[2] or the Stark tuning of molecular transitions.[3] For the latter cases the determination of the transition frequency involves the calibration of the laser frequency or the determination of additional parameters.

It has been found, however, that the line shape of the two-photon Lamb dips changes considerably with experimental conditions.[4] Sometimes observed dips were of a dispersion form, but sometimes they were of a Lorentzian form. In addition, when the radio frequency was within the Doppler width of the molecular transition, many satellite lines were observed.[4]

This paper presents theoretical explanations for those line-shape variations in the two-photon Lamb-dip experiments. The problem is to find the nonlinear susceptibility of a molecular system when optical radiations propagating in opposite directions and a radio-frequency (rf) field are simultaneously applied to the molecules. The configuration is schematically shown in Fig. 1.

The following discussions are based on the standard semiclassical formulation using a density matrix for the molecular system.[5] The molecular level system considered is a three- or two-level system as shown in Fig. 2. The three-level system represents the case of asymmetric-top molecules or inversion-split symmetric-top molecules (such as NH_3) in which each level has a single parity. The two-level system represents the case of symmetric-top molecules with $K \neq 0$ in which each level has a double parity. For this case a finite diagonal dipole matrix element exists. Using classical field, the interactions of wave functions corresponding to these levels through dipole matrix elements are considered.

The procedure to obtain the susceptibility is similar to that for the theory of the gas laser.[6-8] The same theory has also been used for the calculations of nonlinear susceptibilities by many authors.[9] The theory consists of two steps. First, the quantum-mechanical response of molecules which are moving at a particular axial velocity is calculated from the density-matrix equation. The bulk susceptibility of the gas is then obtained by integrating the solution over the velocity distribution. In most cases the Doppler width is assumed to be much larger than the homogeneous width. The basic theoretical formulation is given in Sec. II.

In Sec. III we obtain solutions by using straightforward perturbation techniques. Many of the observed effects are related to only a few terms of the perturbation expansion. Additional effects due to stronger fields are discussed in Sec. IV, where the discussions are limited to the two-level system for simplicity. Major effects are shifts and broadenings of the resonance lines. Some modifications are necessary when the sample cell is placed inside the laser cavity. This is discussed in Sec. V.

II. THEORY

We consider a system of molecules interacting with two optical fields traveling in opposite directions

$$E'_+ e^{-i\omega t+ikz} + E'_- e^{-i\omega t-ikz} + \text{c.c.}, \tag{1}$$

and a rf field

$$E_r e^{-i\omega_r t} + \text{c.c.}$$

The rf field may be either a standing or a traveling wave. Its spatial dependence is ignored, because the Doppler width at radio frequency is usually much smaller than the homogeneous width. This is the case also for the microwave radiation.

Two cases are considered for the molecular-level systems as shown in Fig. 2. In the three-level system shown in Fig. 2(a), the separation between the levels 1 and 2 is in the rf region and the separation between the levels 2 and 3 is in a near coincidence with the optical frequency of a laser. The levels 1-2 and 2-3 are connected by the dipole matrix elements μ_{12} and μ_{23}, respectively. Figure 2(b) represents a two-level system of symmetric-top molecules where each level has a double parity. The levels 2 and 3 are separated by the optical frequency. In addition to the off-diagonal matrix element μ_{23}, there are diagonal dipole matrix elements μ_2 and μ_3 for levels 2 and 3, respectively.

The molecules which move with an axial velocity $-v$ past the point $z=z_0$ at a time $t=t_0$, experience the field

$$E = E_+ e^{-i(\omega+kv)t} + E_- e^{-i(\omega-kv)t} + E_r e^{-i\omega_r t} + \text{c.c.}, \tag{2}$$

where $E_\pm = E'_\pm \exp[\pm ik(vt_0 - z_0)]$. The response of an ensemble of those molecules can be described by the following density-matrix equation:

$$\frac{d\rho'}{dt} = \frac{1}{i\hbar}[H, \rho'] - \Gamma(\rho' - \rho'^{(0)}). \tag{3}$$

In the above equation, the Hamiltonian H is

$$H = \begin{pmatrix} \hbar\omega_{13} & -\mu_{12}E & 0 \\ -\mu_{12}E & \hbar\omega_{23} & -\mu_{23}E \\ 0 & -\mu_{23}E & 0 \end{pmatrix}$$

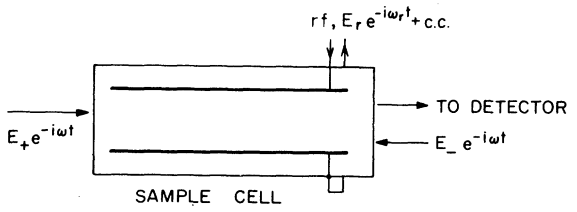

FIG. 1. Schematic experimental configuration.

for the three-level system where $\hbar\omega_{ij}$ is the energy difference between levels i and j. For the two-level system, the Hamiltonian is

$$H = \begin{pmatrix} \hbar\omega_{23} - \mu_2 E & -\mu_{23}E \\ -\mu_{23}E & -\mu_3 E \end{pmatrix}.$$

The second term in Eq. (3) is a phenomenological damping term, where Γ is the matrix of the relaxation rates γ_{ij}. We now factor out the optical-frequency oscillation by substituting off-diagonal matrix elements such as $\rho'_{23} = \rho_{23} e^{-i\omega_{23}t}$, $\rho'_{13} = \rho_{13} e^{-i\omega_{23}t}$, $\rho_{32} = \rho^*_{23}$, and $\rho_{31} = \rho^*_{13}$. For all other elements $\rho'_{ij} = \rho_{ij}$. After dropping all terms which oscillate at optical frequencies, Eq. (3) becomes, for the three-level system,

$$\begin{aligned}
&\left(\frac{d}{dt} + \gamma_r\right)\rho_r = -2iy_r(\rho_{12} - \rho_{21}) + iy_0\rho_{23} - iy_0^*\rho_{32}, \\
&\left(\frac{d}{dt} + \gamma_0\right)\rho_0 = iy_r(\rho_{12} - \rho_{21}) \\
&\qquad\qquad - 2iy_0\rho_{23} + 2iy_0^*\rho_{32} + \gamma_0\rho_0^{(0)}, \\
&\left(\frac{d}{dt} + i\omega_{12} + \gamma_{12}\right)\rho_{12} = -iy_r\rho_r - iy_0\rho_{13}, \\
&\left(\frac{d}{dt} + \gamma_{23}\right)\rho_{23} = iy_r\rho_{13} - iy_0^*\rho_0, \\
&\left(\frac{d}{dt} + i\omega_{12} + \gamma_{13}\right)\rho_{13} = iy_r\rho_{23} - iy_0^*\rho_{12}.
\end{aligned} \tag{4}$$

In Eq. (4), $\rho_r = \rho_{11} - \rho_{22}$, $\rho_0 = \rho_{22} - \rho_{33}$, $y_r = x_r e^{-i\omega_r t} + \text{c.c.}$, and $y_0 = x_+^* e^{i\Omega_+ t} + x_-^* e^{i\Omega_- t}$, where $\Omega_\pm = \Omega \pm u$, $\Omega = \omega - \omega_{23}$, $u = kv$, $x_r = \mu_{12}E_r/\hbar$, and $x_\pm = \mu_{23}E_\pm/\hbar$. For the two-level system we obtain

$$\left(\frac{d}{dt} + \gamma_0\right)\rho_0 = -2iy_0\rho_{23} + 2iy_0^*\rho_{32} + \gamma_0\rho_0^{(0)}, \tag{5a}$$

$$\left(\frac{d}{dt} + \gamma_{23}\right)\rho_{23} = -iy_0^*\rho_0 - iy_d\rho_{23}, \tag{5b}$$

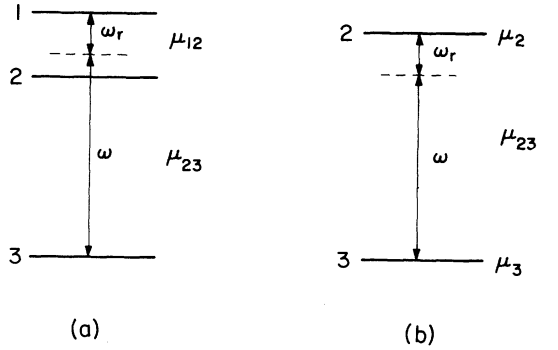

FIG. 2. Molecular energy-level diagrams for a three-level system (a) and for a two-level system (b).

where

$$y_d = (\mu_3 - \mu_2) E_r e^{-i\omega_r t}/\hbar + \text{c.c.}$$
$$= x_r e^{-i\omega_r t} + \text{c.c.}$$

In deriving Eqs. (4) and (5) the diagonal relaxation rates γ_{11}, γ_{22}, and γ_{33} are assumed to be equal and all terms whose oscillating frequencies are in the rf region are retained.

The steady-state solutions of Eqs. (4) or (5) are expressed in a series of terms which oscillate at various frequencies $l\Omega_+ + m\Omega_- + n\omega_r$, where l, m, and n are integers. In order to calculate the susceptibility to E'_+ field, we have only to know the part of $\rho_{23}, \rho_{23}(-\Omega_+)$, whose time dependence is $e^{-i\Omega_+ t}$. In Eqs. (4) and (5), the fields $E_\pm$ and E_r are always accompanied by the factors $e^{-i\Omega_\pm t}$ and $e^{-i\omega_r t}$, respectively. Therefore, it is expected that when ρ_{ij} is expanded in powers of the field, the term with the time dependence of $\exp[i(l\Omega_+ + m\Omega_- + n\omega_r)t]$ will appear with a factor of $E_+^l E_-^m E_r^n |E_+|^{l'} |E_-|^{m'} |E_r|^{n'}$. Thus, one may assume for $\rho_{23}(-\Omega_+)$

$$\rho_{23}(-\Omega_+) = f(v, \Omega, \omega_r, |E_+|^2, |E_-|^2, |E_r|^2) E_+ e^{-i\Omega_+ t},$$

where the function f depends only on the intensities of the fields $|E_\pm|^2 = |E'_\pm|^2$ and $|E_r|^2$. The induced polarization at z_0 and at time t_0 produced by those molecules is then calculated to be

$$\mu_{23} f E'_+ e^{-i(\omega t_0 - kz_0)}.$$

The bulk susceptibility of molecules is obtained by integrating f over the molecular-velocity distribution.

$$\chi = \mu_{23} \int N(v) f \, dv.$$

III. PERTURBATION THEORY

We discuss in this section the solutions of Eqs. (4) and (5) by using the standard perturbation method in which the density matrix ρ is expanded in powers of the three fields E_+, E_-, and E_r as

$$\rho = \rho^{(0)} + \rho^{(1)} + \rho^{(2)} + \cdots.$$

The term $\rho^{(n)}$ is proportional to the nth power of the fields and is obtained from $\rho^{(n-1)}$ by substituting the latter into the right-hand side of Eqs. (4) or (5). In general, $\rho^{(n)}$ is expressed as an n product of factors of the form

$$\frac{\pm ix}{i[l\Omega_+ - (l \pm 1)\Omega_- + m\omega_r] + \gamma}, \tag{6}$$

where x represents $x_\pm$ or x_r and l and m are integers. We pick up the terms with the relevant time dependence $\rho_{23}(-\Omega_+)$ in the series. The susceptibility is then obtained by integrating the expression over v or equivalently over u. For the Dopper-limited case, the integration may be performed to infinity. The integral is obtained by simply summing up residues of all poles existing in either upper or lower complex u plane. The number of terms increases rapidly as we go to higher-order perturbation. However, for specific processes such as those discussed in this paper the number is usually not very large. Furthermore, one can omit any term which has poles only on one side of the real axis, because for such a term the integration over u vanishes.

A. The lowest-order terms

The two-photon Lamb dip is observed as a perturbation on the susceptibility for the E_+ field by E_- and E_r waves. The lowest-order term with such an effect is in the fifth-order solution of Eq. (4) and should be proportional to $x_+ |x_-|^2 |x_r|^2$.

It also has to appear with an expression which is resonant at $\Omega \pm \omega_r$. For $\Omega + \omega_r$ resonance, the only term which does not vanish after the integration is the one that is obtained by the iteration scheme shown in Fig. 3(a):

$$\tilde{\rho}_{23}^{(5)} = \frac{-ix_-}{-i\Omega_- + \gamma_{23}} \frac{ix_r}{-i\Omega_- - i\omega_r + i\omega_{12} + \gamma_{13}} \times \frac{-ix_-^*}{-i\omega_r + i\omega_{12} + \gamma_{12}} \frac{-ix_+}{-i\Omega_+ - i\omega_r + i\omega_{12} + \gamma_{13}} \times \frac{ix_r^*}{-i\Omega_+ + \gamma_{23}} \rho_0^{(0)}.$$

On the left-hand side $\tilde{\rho}_{ij}^{(k)}$ indicates that only the relevant terms in the kth-order expansion $\rho_{ij}^{(k)}$ are picked up. Assuming all γ's are equal, $|\omega_r - \omega_{12}| \gg \gamma$, and $\Omega + \omega_r - \omega_{12} \sim 0$, the integration over u gives

$$\int_{-\infty}^{\infty} \tilde{\rho}_{23}^{(5)} du = \frac{\pi x_+ |x_-|^2 |x_r|^2}{(\omega_r - \omega_{12})^2 (2\Omega + \omega_r - \omega_{12})} \times \frac{i}{(\Omega + \omega_r - \omega_{12}) + i\gamma}. \tag{7}$$

The resonance at $\Omega - \omega_r$ is obtained by replacing ω_r by $-\omega_r$ in Eq. (7). For a two-level system, the iteration scheme is shown in Fig. 3(b). The final result is

$$\int_{-\infty}^{\infty} \tilde{\rho}_{23}^{(5)} du = \frac{2\pi x_+ |x_-|^2 |x_r|^2}{\omega_r^3} \frac{-i}{(\Omega + \omega_r) + i\gamma}. \tag{8}$$

If $\omega_{12} = 0$ and $\Omega + \omega_r \approx 0$, the two expressions (7) and (8) coincide except for a factor of 2. This factor is due to a difference in the definition of the dipole moments. If the two-level system is con-

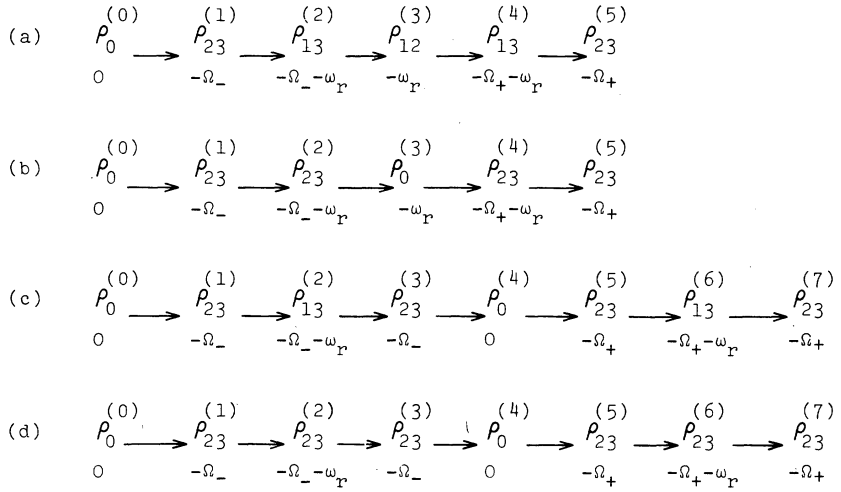

FIG. 3. Iteration processes in the perturbation calculations in Section III A. Letters under $\rho_{jk}^{(i)}$ indicates the frequency components to be calculated. (a) and (b) are the lowest-order terms for three- and two-level systems, respectively. (c) and (d) are the two-photon Lamb dips which are a direct analogy to the normal Lamb dip, for three- and two-level systems, respectively.

sidered as the limiting case of a three-level system with $\omega_{12} \to 0$, the diagonal matrix element μ_2 should be replaced by $\mu_{12}/\sqrt{2}$.

The results of the two-photon Lamb dip given in Eqs. (7) and (8) are considerably different from the normal Lamb dip, which is derived from third-order terms in the perturbation procedure

$$\int_{-\infty}^{\infty} \tilde{\rho}_{23}^{(3)}\, du = \frac{2\pi x_+ |x_-|^2}{\gamma} \frac{-1}{\Omega + i\gamma}. \tag{9}$$

First, the absorption coefficient in Eq. (7) or (8) has the dispersion form, while in Eq. (9) it has the normal Lorentzian shape. This is because the iteration schemes shown in Figs. 3(a) and 3(b) are not straightforward extensions of the case of single-photon Lamb dips to that of "two-photon Lamb dips." For a single-photon Lamb dip, the change in the population difference ρ_0 caused by the absorption of E_- field is observed through the single-photon absorption of E_+ field. The direct extension of this to the two-photon case mechanism will be the observation of the change in ρ_0 caused by the two-photon absorption of E_- and E_r fields, through the two-photon absorption of E_+ and E_r fields. Such effect appears in the seventh-order perturbation. The scheme is shown in Fig. 3(c) for the three-level system and in 3(d) for the two-level system. The results are

$$\int_{-\infty}^{\infty} \tilde{\rho}_{23}^{(7)}\, du = \frac{2\pi x_+ |x_-|^2 |x_r|^4}{(\omega_r - \omega_{12})^2 (2\Omega + \omega_r - \omega_{12})^2 \gamma} \times \frac{-1}{(\Omega + \omega_r - \omega_{12}) + i\gamma}, \tag{10}$$

and

$$\frac{2\pi x_+ |x_-|^2 |x_r|^4}{\omega_r^4 \gamma} \frac{-1}{\Omega + \omega_r + i\gamma} \tag{11}$$

for Figs. 3(c) and 3(d), respectively. The resonance at $\Omega - \omega_r$ is obtained by replacing ω_r by $-\omega_r$. Those terms have the Lorentzian absorption shape as in the single-photon Lamb dip. In Figs. 3(a) and 3(b), in contrast, the induced polarization at ω_r, produced by the Raman process of E_- and E_r, is observed again through the Raman process of E_+ and E_r. Although the seventh-order effect given in Eq. (10) or (11) is of higher order it takes over the fifth-order effect given in Eq. (7) or (8) when $|x_r|^2/\omega_r\gamma > 1$. It will be shown in Sec. IV A that the variations of line shape with E_r is caused mainly by the competition between those two contributions.

In a single-photon Lamb dip, the change in the population becomes appreciable when $|x_\pm| \gtrsim \gamma$. At this field intensity the susceptibility of the Lamb dip is on the same order of magnitude as the linear susceptibility. In the two-photon case, the population change between levels 1 and 3 becomes appreciable when $|x_\pm x_r| \gtrsim \Delta\omega\gamma$, where $\Delta\omega$ is the frequency mismatch at the intermediate state. However, the susceptibility of the two-photon Lamb dip is smaller than the linear susceptibility by a factor of $\gamma/\Delta\omega$ even at this intensity. This is because the observation is done through the intensity change of an off-resonant field E_+. The same reduction in the susceptibility is expected in any nonlinear effect, if the observing field is off-resonant to the molecular transition. This limits the applicability of two-photon technique to cases of larger $\Delta\omega$, because one has to increase the linewidth γ in order to keep the same absorption coefficient, even when the field intensities are sufficiently strong to saturate the two-photon transition. The situation can be improved, if the population change is directly observed. The population change for the two-level system is given from the sixth order term,

$$\int_{-\infty}^{\infty} \tilde{\rho}_0^{(6)}\, du = -\frac{16\pi|x_+|^2|x_-|^2|x_r|^2}{\omega_r^3\gamma}\,\frac{\Omega+\omega_r}{(\Omega+\omega_r)^2+\gamma^2}\,. \tag{12}$$

One of such methods will be to observe selectively the fluorescence from the upper state, which is a two-photon version of Freed and Javan's technique.[10]

B. Nonzero-velocity Lamb dips

Normal Lamb dips are caused by molecules which have zero-velocity components along the propagations of radiation. However, Lamb dips are caused also by molecules with nonzero-velocity molecules when two saturation dips on the longitudinal velocity profile of the molecules coincide. The integration procedure in Sec. III A is to insert u for which $il'\Omega_+ - i(l'\pm1)\Omega_- + im'\omega_r + \gamma = 0$, into expression (6). Therefore, the requirement of having nonzero-velocity Lamb dip is to be able to find coincidences between two saturation dips at velocities $(\pm\Omega - m\omega_r)/(2l\pm1)$ and $(\pm\Omega - m'\omega_r)/(2l'\pm1)$. Since l, m, l', and m' are arbitrary integers, the coincidence can occur at $\omega_r = (2j/n)\Omega$, where j and n are any integers.

If ω_r is much larger than the Doppler width, only the normal dips which correspond to $u=0$, and therefore $m=m'$, are observable. In this case the resonances are restricted to

$$\omega_r = (1/m)\Omega, \quad m = \pm1, \pm2, \ldots .$$

When ω_r is close to or within the Doppler width, coincidences at nonzero velocities become observable. Naturally the lower-order coincidences are stronger. The coincidences, in which one of the saturation dips is due to the two-photon absorption, are shown in Fig. 4. When the rf radiation is intense, the dips corresponding to higher-order multiple rf photon absorption occurs at $u = \Omega - n\omega_r$, $n = 0, 1, 2, \ldots$. The coincidences with the two-photon dip are observed at $\omega_r = (2/n)\Omega$. They are shown by crosses in Fig. 4. If the optical fields are strong, higher-order dips are created at $u = [1/(2n+1)]\Omega$. Resonances due to these dips appear at $\omega_r = [1 \pm 1/(2n+1)]\Omega$, $n = 0, 1, 2, \ldots$, which are shown by circles in Fig. 4. The resonance at $\omega_r = 2\Omega$ is of lower order than the two-photon Lamb dip. Next-strongest resonances are expected at $\omega_r = \frac{2}{3}\Omega$ and $\frac{4}{3}\Omega$, as observed.[6,11]

IV. EFFECT OF HIGHER FIELD

The largest contribution to the nth order $\rho^{(n)}$ is due to the terms which have resonant denominators in each second factor of the iteration process. When $\Omega_\pm \pm \omega_r \sim 0$, those terms have a magnitude of $|x|^{2m}/(\omega_r^m\gamma^m)$ and $|x|^{2m+1}/(\omega_r^{m+1}\gamma^m)$, for even $n=2m$ and odd $n=2m+1$, respectively. Therefore, when the field intensity $|x|^2$ is larger than $\omega_r\gamma$, the perturbation expansion does not converge. The saturation effect starts to appear at such a field intensity. This situation is discussed in the following using the method of solutions which is similar to that of the intense gas laser theory.[7,8] In most general cases the solutions are expressed in terms of fractional series and the evaluation can be done numerically. First we discuss the case when only one of the rf or optical fields is strong. The effects are considerably different for those two cases. Although many of the following results can be applied, in principle, to arbitrarily strong fields, we assume implicitly that $|x|^2 \ll \omega_r^2$. The field intensity such that $|x|^2 \gtrsim \omega_r^2$ is almost impossible to obtain except at the very low ω_r. Furthermore, only the two-level system is considered throughout this section. The three-level system will give qualitatively the same result.

A. Intense rf field

Let us consider the exact solution of Eq. (5b) by taking $g = -iy^*\rho_0$ as a known function. Suppose g has a time dependence of $e^{-i\theta t}$, then ρ_{23} is expressed as a sum

$$\sum_n \rho_{23}(-\theta + n\omega_r)\exp[i(-\theta + n\omega_r)t]\,.$$

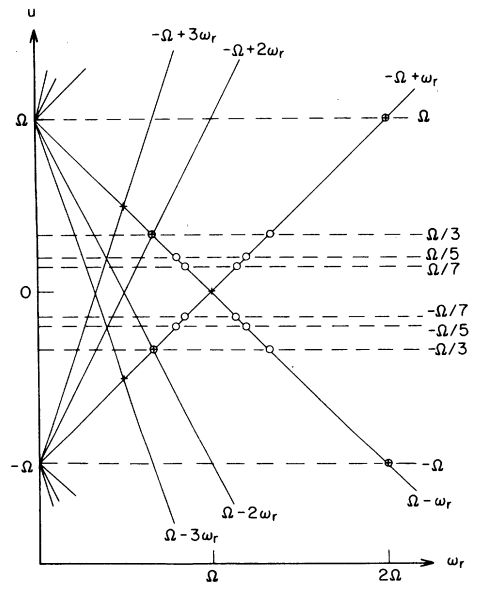

FIG. 4. Higher-order Lamb dips. Circles are coincidences between two-photon saturation dip and higher-order saturation dips caused by the optical fields. Crosses are coincidences between two-photon saturation dip and the dips produced by multiple rf photons and an optical photon. The figure shows only up to third order.

By comparing the coefficients of terms which have the same time dependence, the equations for $\rho_{23}(-\theta+n\omega_r)$ are written in a recurrence form

$$(-i\theta+in\omega_r+\gamma_{23})\rho_{23}(-\theta+n\omega_r) = -ix_r^*\rho_{23}(-\theta+(n+1)\omega_r) - ix_r\rho_{23}[-\theta+(n-1)\omega_r]+g\delta_{n0}.$$

The solution is obtained as a product of fractional series. By defining

$$K_\pm(-\theta) = (-i\theta+\gamma_{23}) + \cfrac{|x_r|^2}{(-i\theta\pm i\omega_r+\gamma_{23}) + \cfrac{|x_r|^2}{(-i\theta\pm 2i\omega_r+\gamma_{23}) + \cfrac{|x_r|^2}{\cdots}}}, \tag{13}$$

and

$$M(-\theta) = (-i\theta+\gamma_{23}) + \frac{|x_r|^2}{K_+(-\theta+\omega_r)} + \frac{|x_r|^2}{K_-(-\theta-\omega_r)},$$

the general solution is

$$\begin{aligned}\rho_{23}(-\theta+n\omega_r) &= \frac{g}{M(-\theta)}\prod_{j=1}^{n}\frac{-ix_r^*}{K_+(-\theta+j\omega_r)} \qquad (n\geq 0),\\ \rho_{23}(-\theta-n\omega_r) &= \frac{g}{M(-\theta)}\prod_{j=1}^{n}\frac{-ix_r}{K_-(-\theta-j\omega_r)} \qquad (n\geq 0).\end{aligned} \tag{14}$$

We seek for the solution whose optical field dependence is $|x_-|^2x_+$. The iteration series is shown in Fig. 5(a). In calculating $\rho_{23}^{(i)}$ from $\rho_0^{(i-1)}$, the expression in Eq. (14) is used instead of the simple perturbation form Eq. (6). This is shown by thick arrows in Fig. 5(a). In the last result $\rho_{23}^{(3)}$, the terms with time dependence $e^{-i\Omega_+ t}$ are picked up. The final result is

$$\begin{aligned}&\frac{-ix_-}{M(-\Omega_-)}\frac{-2ix_-^*}{\gamma_d}\frac{-ix_+}{M(-\Omega_+)} + \sum_{n=1}^{\infty}\left[\frac{-ix_-}{M(-\Omega_-)}\left(\prod_{j=1}^{n}\frac{-ix_r^*}{K_+(-\Omega_-+j\omega_r)}\right)\frac{-2ix_-^*}{in\omega_r+\gamma_d}\frac{-ix_+}{M(-\Omega_++n\omega_r)}\right.\\ &\qquad\times\left(\prod_{j=1}^{n}\frac{-ix_r}{K_-[-\Omega_++(n-j)\omega_r]}\right) + \frac{-ix_-}{M(-\Omega_-)}\left(\prod_{j=1}^{n}\frac{-ix_r}{K_-(-\Omega_--j\omega_r)}\right)\\ &\qquad\left.\times\frac{-2ix_-^*}{-in\omega_r+\gamma_d}\frac{-ix_+}{M(-\Omega_+-n\omega_r)}\left(\prod_{j=1}^{n}\frac{-ix_r^*}{K_+[-\Omega_+-(n-j)\omega_r]}\right)\right].\end{aligned} \tag{15}$$

Equation (15) includes all contributions whose optical field dependence is $|x_-|^2x_+$. When $|x_r|^2 \ll \omega_r^2$, only the first two terms in Eq. (15) have large contributions. Assuming $\Omega+\omega_r\sim 0$, they are

$$\left(\frac{-ix_-}{M(-\Omega_-)}-\frac{-ix_-}{-i\Omega+\gamma_n}\right)\frac{-2ix_-^*}{\gamma_d}\left(\frac{-ix_+}{M(-\Omega_+)}-\frac{-ix_+}{-i\Omega_++\gamma_n}\right)$$

and

$$\frac{-ix_-}{M(-\Omega_-)}\frac{-ix_r}{K_-(-\Omega_--\omega_r)}\frac{-2ix_-^*}{-i\omega_r+\gamma_d}\times\frac{-ix_+}{M(-\Omega_+-\omega_r)}\frac{-ix_r^*}{K_+(-\Omega_+)}.$$

The first expression is derived from the first term in Eq. (15) by deducting lower-order resonance terms. The contribution of other terms is smaller by a factor of at least γ/ω_r. When we further simplify those expressions using the same assumption $|x_r|^2 \ll \omega_r^2$, they become exactly the same as Eqs. (11) and (8), respectively. These results indicate that the main effect of the saturation by intense rf field is to change the line shape from dispersion form to Lorentzian form when $|x_r|^2$ exceeds $\frac{1}{2}\omega_r\gamma$. Neither saturation broadening nor frequency shift appears in Eq. (15).

B. Intense x_- field

Influences of strong optical fields on the line shape are more complicated than the influence of the strong rf field. If only the x_- field is strong, however, the result can be expressed in an algebraic function. This form is obtained by adding all terms with an arbitrary number of factors

$$\frac{-2|x_-|^2}{(-i\Omega'\pm i\Omega_-+\gamma_{23})(-i\Omega'+\gamma_0)},$$

at $\rho_0^{(0)}$, $\rho_0^{(3)}$, $\rho_{23}^{(4)}$, and $\rho_{23}^{(5)}$ in Fig. 3(b), where Ω' stands for 0, ω_r, $\Omega_+\mp\Omega_-+\omega_r$, and $\Omega_+\mp\Omega_-$, respectively. Assuming $|x_-|^2 \ll \omega_r^2$, the fifth-order term becomes

$$\frac{-2x_+|x_-|^2|x_r|^2}{\omega_r^3}\,\frac{1}{-\Omega_- - \omega_r + 2|x_-|^2/\omega_r - i\gamma_{23}}\,\frac{1}{\Omega_+ + \omega_r - 2|x_-|^2/\omega_r + i\gamma_{23}}\left(1 - \frac{2|x_-|^2/\omega_r}{-\Omega_- + \Omega_+ + i\gamma_0}\right).$$

The integration over u gives

$$\frac{-2\pi i x_+|x_-|^2|x_r|^2}{\omega_r^3}\,\frac{1}{\Omega + \omega_r - 2|x_-|^2/\omega_r + i\gamma_{23}}\left(1 - \frac{|x_-|^2/\omega_r}{\Omega + \omega_r - 2|x_-|^2/\omega_r + i(\gamma_{23} + \gamma_0/2)}\right). \tag{16}$$

The line is shifted in frequency by $2|x_-|^2/\omega_r$. At higher intensity $|x_-|^2 > \omega_r\gamma$, the second term in the parentheses become dominant, whose imaginary part is more or less similar to a second derivative of the Lorentzian shape. The linewidth is not affected by x_- field as in the case of intense rf field.

C. Intense x_- and x_+ fields

When both optical fields are strong, one has to include terms with an arbitrary number of factors which contain x_+ and/or x_-. This correction has to be done at three places in Fig. 3(b); $\rho_0^{(0)} \to \rho_{23}^{(1)}$, $\rho_{23}^{(2)} \to \rho_{23}^{(4)}$, and at $\rho_{23}^{(5)}$. However, it can be shown that in the first and the last corrections only a finite number of terms are important, as long as $|x_\pm|^2 \ll \omega_r^2$. The iteration processes are shown in Fig. 5(b). The box indicates the infinite sum in $\rho_{23}^{(2)} \to \rho_{23}^{(4)}$. This summation is equivalent to solve Eqs. (5) with $y_d = 0$ and

$$\rho_0^{(0)} = \sum_n \rho_0^{(3)}(-n\Delta\Omega - \omega_r)\exp[-i(n\Delta\Omega + \omega_r)t],$$

where $\Delta\Omega = \Omega_+ - \Omega_- = 2u$. The comparison of the coefficients for the same frequency components gives

$$\left(-in\Delta\Omega - i\omega_r + \gamma_0 + \frac{4|x_+|^2(\gamma_{23} - in\Delta\Omega - i\omega_r)}{\Omega_+^2 + (\gamma_{23} - in\Delta\Omega - i\omega_r)^2} + \frac{4|x_-|^2(\gamma_{23} - in\Delta\Omega - i\omega_r)}{\Omega_-^2 + (\gamma_{23} - in\Delta\Omega - i\omega_r)^2}\right)\rho_0^{(4)}(-n\Delta\Omega - \omega_r)$$
$$+ 2x_+^* x_-\left(\frac{1}{i\Omega_+ - in\Delta\Omega - i\omega_r + \gamma_{23}} + \frac{1}{-i\Omega_- - in\Delta\Omega - i\omega_r + \gamma_{23}}\right)\rho_0^{(4)}[-(n-1)\Delta\Omega - \omega_r]$$
$$+ 2x_+ x_-^*\left(\frac{1}{-i\Omega_+ - in\Delta\Omega - i\omega_r + \gamma_{23}} + \frac{1}{i\Omega_- - in\Delta\Omega - i\omega_r + \gamma_{23}}\right)\rho_0^{(4)}[-(n+1)\Delta\Omega - \omega_r] = \gamma_0\rho_0^{(3)}(-n\Delta\Omega - \omega_r). \tag{17}$$

The susceptibility is obtained from the integration of the sum

$$\rho_{23}^{(6)}(-\Omega_+) + \rho_{23}^{(8)}(-\Omega_+) \tag{18}$$

in Fig. 5(b). Equation (17) can be calculated numerically by truncating at a finite number n. However, the convergence in Eq. (17) is rather slow when u is small and $|x_\pm|^2$ are large. Particularly when $u = 0$, and $|x_+| = |x_-|$,

$$\left|\frac{\rho_{23}^{(4)}(-(n+1)\Delta\Omega - \omega_r)}{\rho_{23}^{(4)}(-n\Delta\Omega - \omega_r)}\right| \approx \left|1 \pm \left(\frac{-\omega_r(\omega_r + \Omega - i\gamma_{23})}{2|x_\pm|^2}\right)^{1/2}\right|.$$

Therefore, a relatively large number of $\rho_{23}^{(4)}(-n\Delta\Omega - \omega_r)$ has to be included in the calculation. Actual numerical solutions show that the first three terms give sufficiently good approximation if $|x_\pm|^2 \lesssim \omega_r\gamma$. In this case the approximate feature of the line shape can be estimated from the

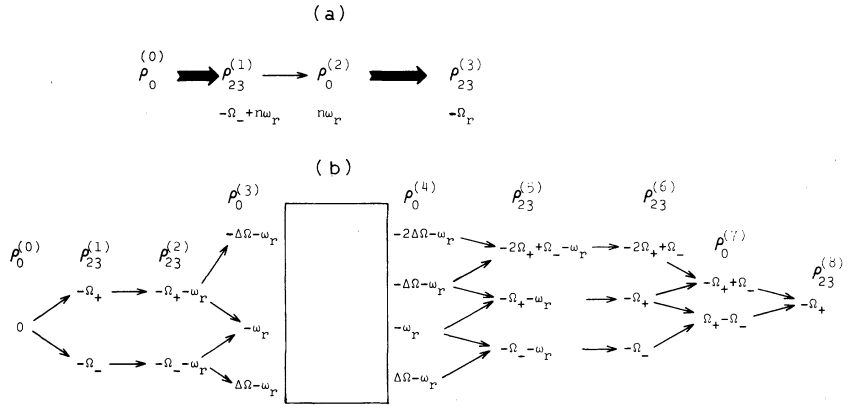

FIG. 5. Iteration processes for intense rf field (a) and for intense optical fields (b). The thick arrows implies infinite sum of terms which have x_r (see Sec. IV A). The box implies infinite sum of terms which have $x_\pm$ (see Sec. IV C).

position of the poles in the solution of Eq. (17). They are

$$\pm\left[\left(\omega_r+\Omega-\frac{2|x_+|^2+2|x_-|^2}{\omega_r}+i\gamma\right)^2-\frac{4|x_+|^2|x_-|^2}{\omega_r^2}\right]^{1/2}. \tag{19}$$

This shows that the line is shifted by $2(|x_+|^2+|x_-|^2)/\omega_r$ and that it has an additional width of the order of $2|x_+x_-|/\omega_r$. The result of the actual calculations shown in Fig. 6 qualitatively agrees with Eq. (19). In Fig. 6 the Doppler width is taken to be 100 times the size of the homogeneous width γ. Figure 6(a) is the weak-field case, which agrees with the perturbation solution in Sec. III A. When the fields intensities are increased the shift and the broadening of the line is seen as in Fig. 6(b). Note that the relative magnitude of the imaginary part decreases while that of the real part keeps increasing. If only the x_- field is large, the linewidth is about the same as in the weak-field case as shown in Fig. 6(c), although the line shift remains. For higher-field intensities Eq. (19) produces a doublet. However, the results of the numerical calculations showed no sign of doublet structures within $|x_\pm|^2 \lesssim 3\omega_r\gamma$. The shift of the amount of $2(|x_+|^2+|x_-|^2)/\omega_r$ exists, but the line shape remains close to that of Fig. 6(b). The doublet in Eq. (19) is probably due to the artificial cutoff of an infinite series, though a doublet structure is experimentally observed in a ν_2 transition in phosphine.[11] The observation may be attributed to the difference in the shift for different M transitions.

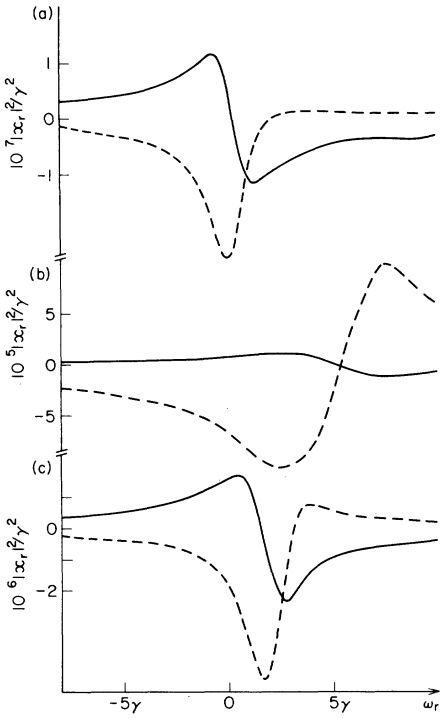

FIG. 6. Real (broken lines) and imaginary (solid lines) parts of the susceptibilities for relatively strong optical fields, the calculations based on the discussions in Sec. IV C. The Doppler width is 100γ, and ω_r is $10^4\gamma$. The vertical scale is normalized to the real part of the linear susceptibility at two-photon resonance. (a) applies to relatively weak fields, $|x_\pm|=|x_-|=25\gamma$; (b) to stronger fields, $|x_+|=|x_-|=100\gamma$; and (c) applies when only x_- is strong, $|x_+|=25\gamma$ and $|x_-|=100\gamma$.

D. General solution

So far the discussions are limited to the case when only one of either the optical or the rf field is strong. The procedures in these discussions are basically to sum infinite terms with factors $|x_j|^{2n}$, $n=0,1,2,\ldots$, for a strong field x_j, while keeping the exponents for the other fields to a finite number. The range of validity for this approximation is not immediately clear, because there is always some N for which $\alpha=|x_i|^2|x_j|^{2N}/(\omega_r\gamma)^{N+1}>1$ as long as $|x_j|^2>\omega_r\gamma$, even if $|x_i|^2$

TABLE I. Matrix components in Eq. (20).

$$A_n\rho_d^{(n-1,l)}+B_n\rho_d^{(n,l)}+C_n\rho_d^{(n+1,l)}=\gamma_d\rho_d^{(0,0)}\delta_{n,0}$$

Definitions:

$$\rho_d^{(n,l)}\propto\exp[(-in\Delta\Omega+il\omega_r)t],\quad \Delta\Omega=\Omega_+-\Omega_-,$$

$$K_\pm(\theta)=(i\theta+\gamma_n)+\cfrac{|x_r|^2}{(i\theta\pm i\omega_r+\gamma_n)+\cfrac{|x_r|^2}{(i\theta\pm 2i\omega_r+\gamma_n)+\cfrac{|x_r|^2}{\cdots}}},$$

$$M(\theta)=i\theta+\gamma_n+\frac{|x_r|^2}{K_+(\theta+\omega_r)}+\frac{|x_r|^2}{K_-(\theta-\omega_r)},$$

$$L_\pm(n;l+m,l)=\frac{1}{M(-n\Delta\Omega\mp\Omega_\pm+l\omega_r)}\times\prod_{j=1}^{m}\frac{\mp ix_r^*}{K_+[-n\Delta\Omega\mp\Omega_\pm+(l+j)\omega_r]},$$

$$L_\pm(n;l-m,l)=\frac{1}{M(-n\Delta\Omega\mp\Omega_\pm+l\omega_r)}\times\prod_{j=1}^{m}\frac{\mp ix_r}{K_-[-n\Delta\Omega\mp\Omega_\pm+(l-j)\omega_r]},\qquad (m\geq 0).$$

Matrix Elements:

$$A_n(l',l)=2x_+x_\pm^*[L_+(n-1;l',l)+L_-(n-1;l',l)],$$

$$B_n(l',l)=(-in\Delta\Omega+il\omega_r+\gamma_d)\delta_{l',l}+2|x_+|^2[L_+(n;l',l)+L_-(n-1;l',l)]+2|x_-|^2[L_+(n-1;l',l)+L_-(n;l',l)],$$

$$C_n(l',l)=2x_\mp^*x_-[L_+(n;l',l)+L_-(n;l',l)].$$

Final:

$$\rho_{12}(-\Omega_+)=-ix_+L_+(0;0,l)\rho_d^{(0,l)}-ix_-L_+(0;0,l)\rho_d^{(1,l)}.$$

$\ll \omega_r\gamma$. Therefore, the above factor α creates a new divergent series of terms which contain an arbitrary exponent of weak field x_i. One can argue that α is always smaller than the term with $|x_j|^{2N}/(\omega_r\gamma)^N$ which is included in the calculation. Sample numerical calculations of the following general formula indicate that the results in Secs. IV A–IV C are good approximations at least when $|x_i x_j| \lesssim \omega_r\gamma$.

For a more accurate treatment, a recurrence formula which is equivalent to Eq. (5) and is convenient for numerical calculations can be obtained using Eq. (14) as the solution of the second equation. Since ρ_0 is related to two frequencies $\Delta\Omega$ and ω_r, it is written in a matrix form

$$A_n \rho_0^{(n-1,)} + B_n \rho_0^{(n,)} + C_n \rho_0^{(n+1,)} = \rho^{(0)} \delta_{n0}, \qquad (20)$$

where $\rho_0^{(n,)}$ is a vector of the components $\rho_0^{(n,l)}$, which oscillates at $-n\Delta\Omega + l\omega_r$. The elements of the matrices A_n, B_n, and C_n are summarized in Table I. Exact numerical calculation is rather complicated, because of the complex matrix form. The solution of Eq. (20) includes contributions from all orders including linear absorption and dispersion. Since the Doppler width is taken to be finite in the numerical calculation, the nonresonant linear effect is usually by far the largest contribution in the result. Therefore, it is also difficult to calculate the weak-field case. When $|x|^2 \sim \omega_r\gamma$, few terms in both $\Delta\Omega$ and ω_r iterations are necessary, and they have appreciable magnitudes.

Figure 7 shows the results for $|x|^2 \sim \omega_r\gamma$, in which the linear response is substracted beforehand. The Doppler width is chosen as 100γ. For the upper two figures only three terms are included in the expression. For the bottom curve seven terms are included. The accuracy is probably better than 5%, which is estimated from the results with different approximations. The result is qualitatively similar to the case of strong optical fields. Both line shift and broadening are observed. However, no complicated structures were found in this intensity range.

V. INTRACAVITY MEASUREMENT

In the experimental configuration shown in Fig. 1, the imaginary part of the susceptibility is measured. However, in the actual experiments the sample cell was usually placed inside the cavity.[1,4] Although this improves the sensitivity, it also complicates the line shape.

The round trip gain G of a homogeneously broadened gas laser may be written approximately as[12]

$$G = \frac{(\Omega' + i\gamma_1)\gamma_1}{[(\Omega'^2 + \gamma_1^2 + 8|x|^2)(\Omega'^2 + \gamma_1^2)]^{1/2}} G_0, \qquad (21)$$

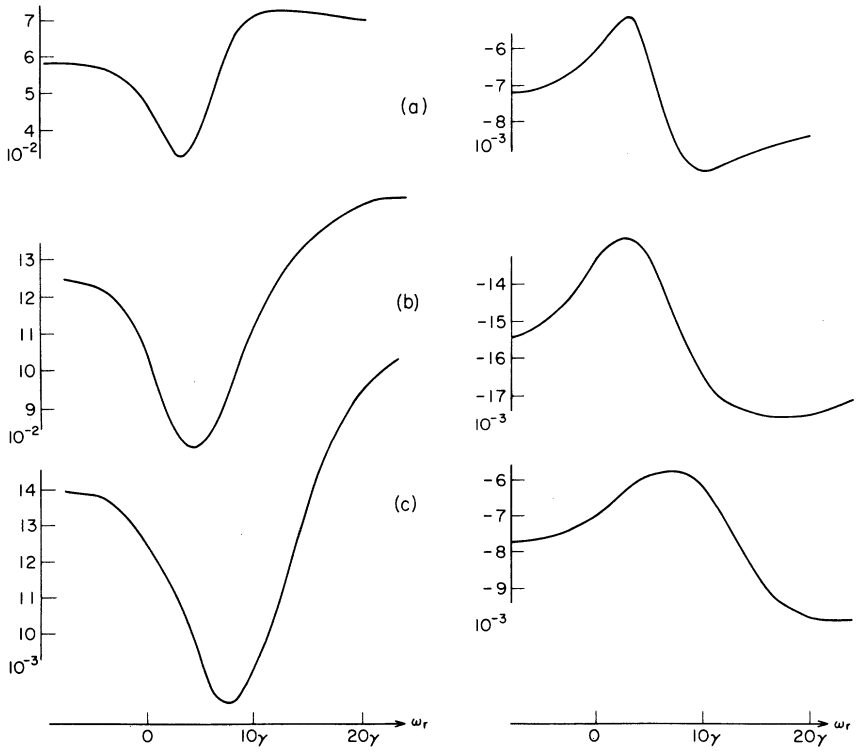

FIG. 7. Real (left) and imaginary (right) parts of the susceptibilities for relatively strong rf and optical fields. The Doppler width is 100γ, and ω_r is $10^4\gamma$. The vertical scale is normalized to the real part of the linear susceptibility at the resonance. (a) $|x_+| = |x_-| = |x_r| = 100\gamma$; (b) $|x_+| = |x_-| = 100\gamma$, $|x_r| = 200\gamma$; (c) $|x_+| = |x_-| = |x_r| = 150\gamma$. The real parts are scaled up to 10 times. The linear responses are deducted.

where $|x| = |x_\pm|$, γ_l is the relaxation rate of the laser levels, and G_0 is the gain at zero off-set frequency $\Omega' = 0$. The laser intensity $|x|^2$ and the oscillation frequency is determined by equating the real and imaginary part of G with the round trip phase shift $\eta = \eta_l + \eta_m$ and the loss factor $\zeta = \zeta_l + \zeta_m$, due to the laser cavity (subscript l) and the sample molecules (subscript m), respectively. This leads to the familiar equation for the frequency pulling

$$\eta/\Omega' = \zeta/\gamma_l ,$$

and the equation for the laser power

$$|x|^2 = \frac{\gamma_l^2}{8}\left(\frac{G_0^2}{\eta^2+\zeta^2} - \frac{\eta^2}{\zeta^2} - 1\right) .$$

It is clear from this equation that the intensity change is proportional to the imaginary part of the susceptibility, only when the cavity mismatch η_l is zero and when the cavity loss is much larger than the absorption by the sample. If the cavity mismatch is not zero, observed intensity change is proportional to a weighted sum of the real and imaginary part of the susceptibility. One can deliberately detune the cavity to measure the real part of the susceptibility. Since the sign of the real part changes with the sign of $\Omega = \omega - \omega_{23}$, the line shape determines which one of the two possible resonances $\omega_{23} = \omega \pm \omega_r$ is being observed.

VI. CONCLUSION

In this paper we have discussed line-shape variations of the two-photon Lamb dip under various experimental conditions. When the rf intensity is changed, the line shape is determined by the competition of two elementary processes. When the optical intensities are increased, the line shifts as well as broadening is expected even if the rf intensity is very weak. The result from the numerical calculations show that the increase in optical intensity beyond the saturation point $|x_\pm|^2 \sim \omega_r\gamma$ only makes the observation more difficult. These results indicate that considerable care has to be taken for the accurate determination of the resonance frequency ω_{23}. The signal intensity dependence of γ/ω_r at optimum field intensities imposes a limitation of this method for higher radio frequency, although the limitation may be partially removed by introduction of other techniques as fluorescence measurement. It should be remembered, however, that this complexity is not particular for the two-photon Lamb dip. Almost all high-order nonlinear effects suffer similar complexities.

ACKNOWLEDGMENTS

The author is grateful to T. Oka and M. Römheld for making their experimental results available to him prior to publication and for stimulating discussions.

---

*Visiting scientist, summer 1973; permanent address: Applied Physics Department, University of Tokyo, Tokyo, Japan.

[1]S. M. Freund and T. Oka, Appl. Phys. Lett. 21, 60 (1972).
[2]T. W. Hänsch, I. S. Shahin, and A. L. Schawlow, Phys. Rev. Lett. 27, 707 (1971).
[3]R. G. Brewer, M. J. Kelley, and A. Javan, Phys. Rev. Lett. 23, 559 (1969).
[4]T. Oka and M. Römheld (private communication).
[5]See for example, A. Javan, Phys. Rev. 107, 1579 (1957).
[6]W. E. Lamb, Jr., Phys. Rev. 134, A1429 (1964).
[7]S. Stenholm and W. E. Lamb, Jr., Phys. Rev. 181, 618 (1969).
[8]B. J. Feldman and M. S. Feld, Phys. Rev. A 1, 1375 (1970).
[9]B. J. Feldman and M. S. Feld, Phys. Rev. A 5, 899 (1972) and references therein.
[10]C. Freed and A. Javan, Appl. Phys. Lett. 17, 53 (1970).
[11]T. Oka, *Laser Spectroscopy*, July, 1973, Vail, Colorado (unpublished).
[12]This is obtained by spacially averaging the response $[(i\Omega+\gamma)\gamma/(\Omega^2+\gamma^2+4|x|^2)]G_0$.